NOTES AND CORRESPONDENCE

Comparison of Ocean Surface Solar Irradiance in the GLA General Circulation Model and Satellite-based Calculations

BETH CHERTOCK

Wave Propagation Laboratory, NOAA/Environmental Research Laboratories, Boulder, Colorado

Y. C. SUD

Laboratory for Atmospheres, NASA/Goddard Space Flight Center, Greenbelt, Maryland

24 June 1991 and 26 May 1992

ABSTRACT

A global, 7-year satellite-based record of ocean surface solar irradiance (SSI) is used to assess the realism of ocean SSI simulated by the nine-layer Goddard Laboratory for Atmospheres (GLA) General Circulation Model (GCM). January and July climatologies of net SSI produced by the model are compared with corresponding satellite climatologies for the world oceans between 54°N and 54°S. This comparison of climatologies indicates areas of strengths and weaknesses in the GCM treatment of cloud–radiation interactions, the major source of model uncertainty. Realism of ocean SSI is also important for applications such as incorporating the GLA GCM into a coupled ocean–atmosphere GCM. The results show that the GLA GCM simulates too much SSI in the extratropics and too little in the tropics, especially in the summer hemisphere. These discrepancies reach magnitudes of 60 W m^{-2} and more. The discrepancies are particularly large in the July case off the western coast of North America. In this region of persistent marine stratus, the GCM climatological values exceed the satellite climatological values by as much as 131 W m^{-2}. Positive and negative discrepancies in SSI are shown to be consistent with discrepancies in planetary albedo.

1. Introduction

A global record of ocean surface solar irradiance (SSI) derived from seven years of satellite observations was used in this study to assess the accuracy of ocean SSI simulated by the nine-layer Goddard Laboratory for Atmospheres (GLA) General Circulation Model (GCM). The resulting analysis of model biases in the net flux of solar radiation absorbed by the ocean, though unimportant for the surface energy balance in an atmospheric GCM in which sea surface temperature (SST) is prescribed (such as the GLA GCM), is nevertheless critically important because it clearly shows deficiencies in the cloud–radiation interaction parameterization. This parameterization constitutes the single greatest source of model uncertainty, and its deficiencies relate directly to the treatment of clouds (e.g., optical thickness and cloud fractions), as well as the treatment of water vapor and absorption by trace gases.

Sud et al. (1990) compared the surface radiation balance for an ensemble of simulations with and without a simple biosphere (SiB) in the GLA GCM. There were some large differences in SSI between the simulations with and without the SiB, but the authors concluded that it was not possible to determine whether the change was an improvement or not. Such a determination requires a comparison of the model climatology with observations or psuedo-observations that have been validated.

With these considerations in mind, we used a satellite-based record of ocean SSI to assess the realism of ocean SSI simulated by the nine-layer GLA GCM in an ensemble of SiB runs. GCM climatologies of ocean SSI for January and July were compared with corresponding satellite-based climatologies. Additional information was provided by a comparison of January and July climatologies of planetary albedo. This is the first time that a satellite-based climatology of ocean SSI for the world oceans has been used to validate SSI simulated by a GCM. Prior to the availability of this satellite dataset (Chertock 1989; Frouin and Chertock 1992; Chertock et al. 1992), the only existing observational climatologies of ocean SSI providing large-scale, long-term coverage were based on ship observations and empirical formulas (e.g., Budyko 1963; Wyrtki 1965; Hastenrath and Lamb 1978; Esbensen and Kushnir 1981; Weare et al. 1981; Hsiung 1986). The ship observations that are used as inputs to the

Corresponding author address: Dr. Beth Chertock, NOAA/Environmental Research Laboratories, Wave Propagation Laboratory, 325 Broadway, Boulder, CO 80303-3328.

empirical parameterizations should not be confused with direct shipboard measurements of the radiative flux. Rather, the empirical formulas require a knowledge of more readily observed quantities such as fractional cloud cover that are routinely recorded aboard both research and nonresearch vessels; GCM validation studies were not feasible because the SSI data generated using these formulas are of questionable accuracy. Therefore, the results of this investigation present a unique evaluation of GLA GCM accuracy as well as an opportunity for future reductions in model error.

The following section contains a description of the version of the GLA GCM used to generate the ocean SSI and planetary albedo climatologies. A description of the corresponding satellite climatologies is given in section 3. The satellite and GCM climatologies are compared in section 4, and these results are discussed in section 5.

2. General circulation model

The GLA GCM, formerly referred to as the Goddard Laboratory for Atmospheric Sciences (GLAS) fourth-order GCM, is documented by Kalnay et al. (1983a,b,c). The horizontal resolution of the model is 4° latitude by 5° longitude. In the vertical, the model has nine sigma layers of equal thickness between 10 mb (the top of the atmosphere) and the surface. There are seven prognostic variables, and the flux forms of the equations of motion are solved using the Euler backward scheme time integration (Matsuno 1966) and fourth-order finite difference equations in space. Boundary conditions (e.g., SST climatology) are externally prescribed, and their seasonal variation is included by interpolation of monthly data once a day at 0000 UTC.

We used an improved version of the GLA GCM with several modifications to the physical parameterizations (Sud et al. 1990). This version incorporates the longwave parameterization of Wu (1980) and the shortwave parameterizations of Lacis and Hansen (1974) and Chou (1986), which were all modified by Sud and Molod (1988) to allow fractional cloud–radiation interaction. The model predicts fractional cloudiness following the method of Slingo and Ritter (1985). The Arakawa–Schubert (1974) parameterization for cumulus clouds was added, along with the modifications of Sud and Molod (1988) to account for the evaporation from falling convective rain. New parameterizations for dry and moist convective mixing processes and an internally consistent determination of large-scale rain were also added. The SiB model of Sellers et al. (1986) was integrated into the GCM to parameterize the fluxes of heat, momentum, and moisture between the atmosphere and vegetation or bare soil. Adding SiB increased the total number of prognostic variables from 7 to 15. The SiB model also required the external prescription of monthly mean vegetation parameters (see Dorman and Sellers 1989) and the partitioning of the solar radiation into components. Although SiB runs have the same marine boundary-layer parameterization as noSiB (i.e., GLA GCM without the SiB model) runs, the implementation of the SiB model introduces changes into the ocean surface fluxes because of air–land interaction effects on the large-scale wind, temperature, and humidity fields.

Four 47-day simulations were run for the model period mid-December through January and for the model period mid-June through July. The boundary conditions were set according to long-term climatological means, and the first 15 days of each run were ignored to allow spin-up time from initial conditions. Therefore, although a given model run does not correspond to a specific month in the observational record, the four January and four July simulations represent the natural variability of the simulated fields in the model atmosphere, and the January and July means represent the respective climatologies.

3. Observational data

Recently, a method was developed and used to generate the first long-term, satellite-based record of ocean SSI for the world oceans (Chertock 1989; Chertock et al. 1991; Frouin and Chertock 1992; Chertock et al. 1992). In this technique, the solar irradiance at the ocean surface is computed from the solar irradiance at the top of the atmosphere by subtracting the solar radiation reflected by the ocean–atmosphere system and subtracting the solar radiation absorbed by atmospheric constituents.

The first of these terms, the solar irradiance at the top of the atmosphere, is a known quantity that is easily calculated according to the astronomical earth–sun configuration. Although not done in the present case, it can also be measured using satellite radiometers. The second term, the solar radiation reflected by the ocean–atmosphere system, is obtained using satellite radiometers. The required information is taken from satellite records of the planetary albedo, that is, the fractional percentage of the incoming solar radiation that is reflected by the planetary system back into space. The data used to generate the new record were *Nimbus-7* satellite wide-field-of-view planetary albedo data from the Earth Radiation Budget (ERB) instrument package. These broadband data cover the 0.2–3.8-μm spectral range. The calibration procedures used to process the data are outlined by Chertock (1989), and details are given by Kyle et al. (1985). The third and final term is the net amount of solar radiation absorbed by atmospheric constituents. This information cannot be obtained from existing direct measurements; therefore, it is obtained theoretically. The planetary atmosphere is modeled as a clear-sky atmosphere positioned above an effective cloud layer, using plane-parallel theory and

assuming the isotropy of radiance reflected by clouds and the surface. The dominant model input parameters are the solar zenith angle, which is calculated exactly, and the planetary albedo, which is taken from satellite observations. The other model input parameters (aerosol type, cloud absorptance, ozone and water vapor amounts, and surface visibility) are set at climatological values.

The net SSI data generated in this manner are monthly mean values that cover the world oceans from November 1978 through October 1985 on a 9° latitude by 9° longitude spatial grid. In situ measurements of SSI over ocean are rare (i.e., limited to the domain of field experiments), and therefore the accuracy of the new global, long-term record could not be verified against in situ measurements directly. However, the new record was verified against in situ measurements indirectly, through comparisons with several high-resolution satellite datasets (Gautier 1986; Gautier et al. 1986; Gautier 1988; Arino 1990) that had previously been verified using in situ measurements taken during field experiments. A sample of the analysis from Chertock et al. (1992) that was used to verify the new dataset against high-resolution satellite datasets is given in Table 1. The validation datasets listed in the table were all generated using the method of Gautier et al. (1980) with radiance measurements from the Visible and Infrared Spin Scan Radiometer (VISSR) aboard Geostationery Operational Environmental Satellite (GOES) series satellites and are associated with the Tropical Ocean–Global Atmosphere (TOGA), Tropic Heat, and Monsoon Experiment (MONEX) field experiments. The Gautier et al. (1980) method is accurate to within 9% on daily time scales and is more accurate on monthly time scales (see Table 2 in Chertock et al. 1992). The TOGA data provide coverage at 32-km by 32-km resolution in the eastern tropical Pacific Ocean (20°N–20°S, 80°W–180°) for January 1980 through September 1983. The Tropic Heat data provide coverage at 32-km by 32-km resolution in the central equatorial Pacific Ocean (5°N–10°S, 110°–150°W) for October 1983 through October 1985. The MONEX data provide coverage at 4-km by 4-km resolution in the Indian Ocean (30°N–20°S, 30°–100°E) for May through July 1979. The VISSR-based datasets were averaged from the original spatial resolution to the 9° latitude by 9° longitude grid of the new ERB-based dataset for the validation study. Although coarser in spatial resolution, the satellite dataset used in this study provides global, long-term coverage, whereas the high-resolution satellite datasets are restricted in both spatial and temporal coverage. On the basis of the analysis presented by Chertock et al. (1992) involving the high-resolution satellite datasets, errors in the new monthly mean record were estimated to lie between 10 and 20 W m^{-2}.

4. Results

January and July monthly means were obtained for the GLA GCM by ignoring the first 15 days and then averaging the remaining 12-h mean values recorded during the integration of each 47-day simulation. January and July model climatologies of ocean SSI (Figs. 1a and 2a, respectively) were computed as the average for the four runs in the ensemble. The analysis is restricted to latitudes between 54°N and 54°S to avoid grid cells with ice background conditions. January and July satellite climatologies were obtained from the observational record by computing the 7-year mean in each case (Figs. 1b and 2b, respectively). The satellite climatologies were subtracted from the corresponding GCM climatologies to produce difference fields for January (Fig. 1c) and July (Fig. 2c). The statistical significance of the differences between the GCM and satellite climatologies was verified using the Student's *t*-test and is indicated in Figs. 1c (January) and 2c (July). In these figures, grid cells are shaded if the mean differences, scaled with the pooled variability of the ensemble, are significant at the 99% level. The zonal means of each 9° latitude band in the GCM and satellite climatologies were computed for January (Fig. 3) and July (Fig. 4). The differences obtained by subtracting the zonal means of the satellite climatologies from the zonal means of the GCM climatologies are shown in Fig. 5. Positive and negative discrepancies in the January and July climatologies were also computed for planetary albedo. The differences between the GCM

TABLE 1. Results of three linear regression analyses for ERB-based surface solar irradiances and corresponding VISSR-based surface solar irradiances in the TOGA, Tropic Heat, and MONEX datasets (from Chertock et al. 1992).

	TOGA	Tropic Heat	MONEX
Number of points	1935	58	43
Slope	0.97	0.996	0.91
Intercept	3.11	2.45	6.66
Linear correlation coefficient, *r*	0.90	0.93	0.95
Rms difference (W m^{-2})	14.45	6.44	16.77
Rms difference (% of mean)	6.2	2.5	7.5
Mean difference* (W m^{-2})	−4.97	1.47	−14.41

* ERB-based minus VISSR-based.

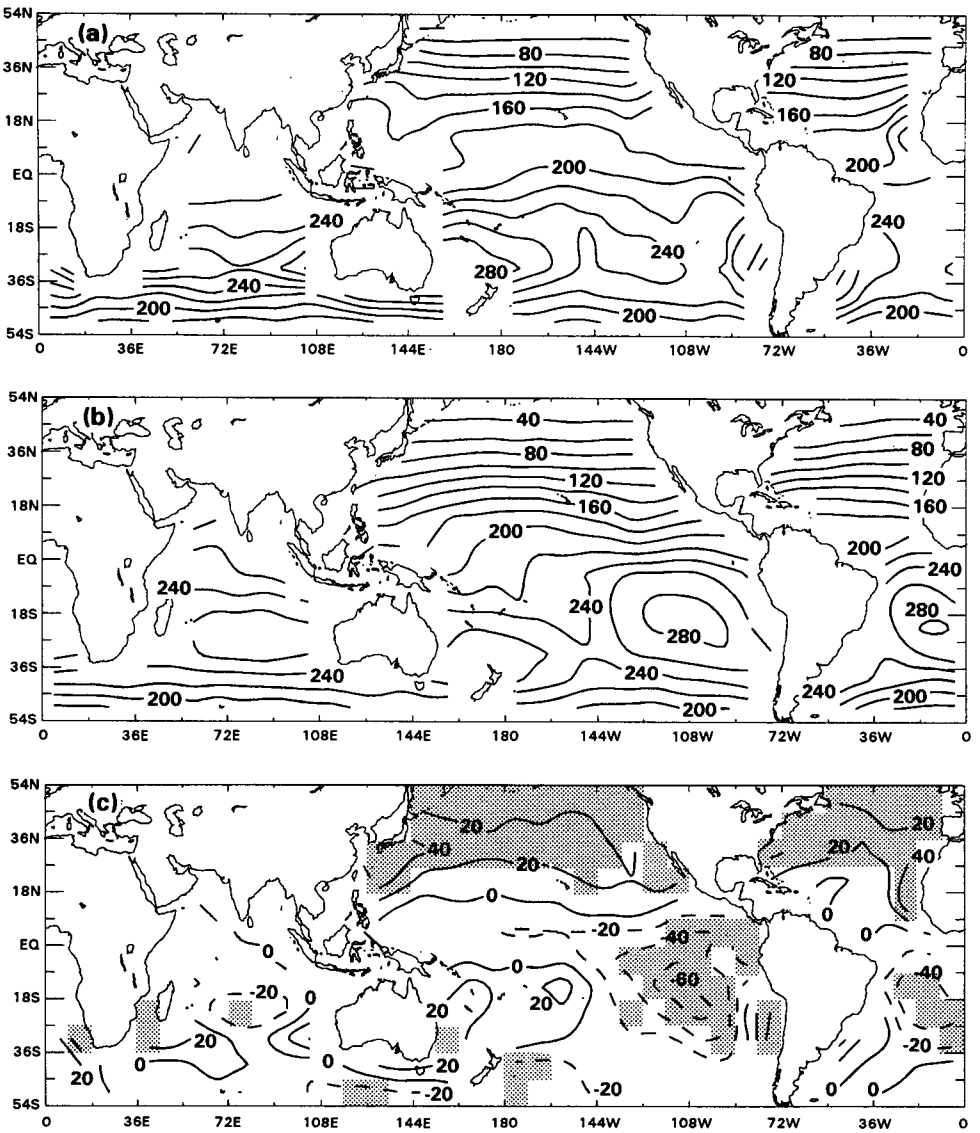

FIG. 1. January climatology of net surface solar irradiance (W m^{-2}) for (a) the GLA GCM and (b) the satellite-based record. The difference field obtained by subtracting (b) from (a) is shown in (c), with negative contours dashed. In (c) shading is used to indicate that the mean differences, scaled with the pooled variability of the ensemble, are significant at the 99% level according to the results of a Student's *t*-test. In each figure the contour interval is 20 W m^{-2}.

climatological values and those from the *Nimbus-7* record discussed in section 3 are shown in Figs. 6a (January) and 6b (July). As in Figs. 1c and 2c, shading is used to indicate that the mean differences, scaled with the pooled variability of the ensemble, are significant at the 99% level according to the results of a Student's *t*-test.

The January climatologies of ocean SSI from the GCM (Fig. 1a) and the satellite dataset (Fig. 1b) display similar gradients and magnitudes in the winter hemisphere (also Figs. 3 and 5). However, the GCM climatological values consistently exceed the satellite climatological values throughout the extratropics of this hemisphere by a statistically significant amount (Fig. 1c). In the summer hemisphere, the two climatologies again display similar zonal gradients, but on zonal average the GCM climatological values for the most part fall below the satellite climatological values (Figs. 3 and 5). These negative discrepancies are statistically significant (Fig. 1c), reaching magnitudes as high as 67 W m^{-2} in the summer hemisphere tropics. The discrepancies in planetary albedo (Fig. 6a) reach their largest positive magnitudes in the specific regions of maximum negative SSI discrepancies. This is consistent

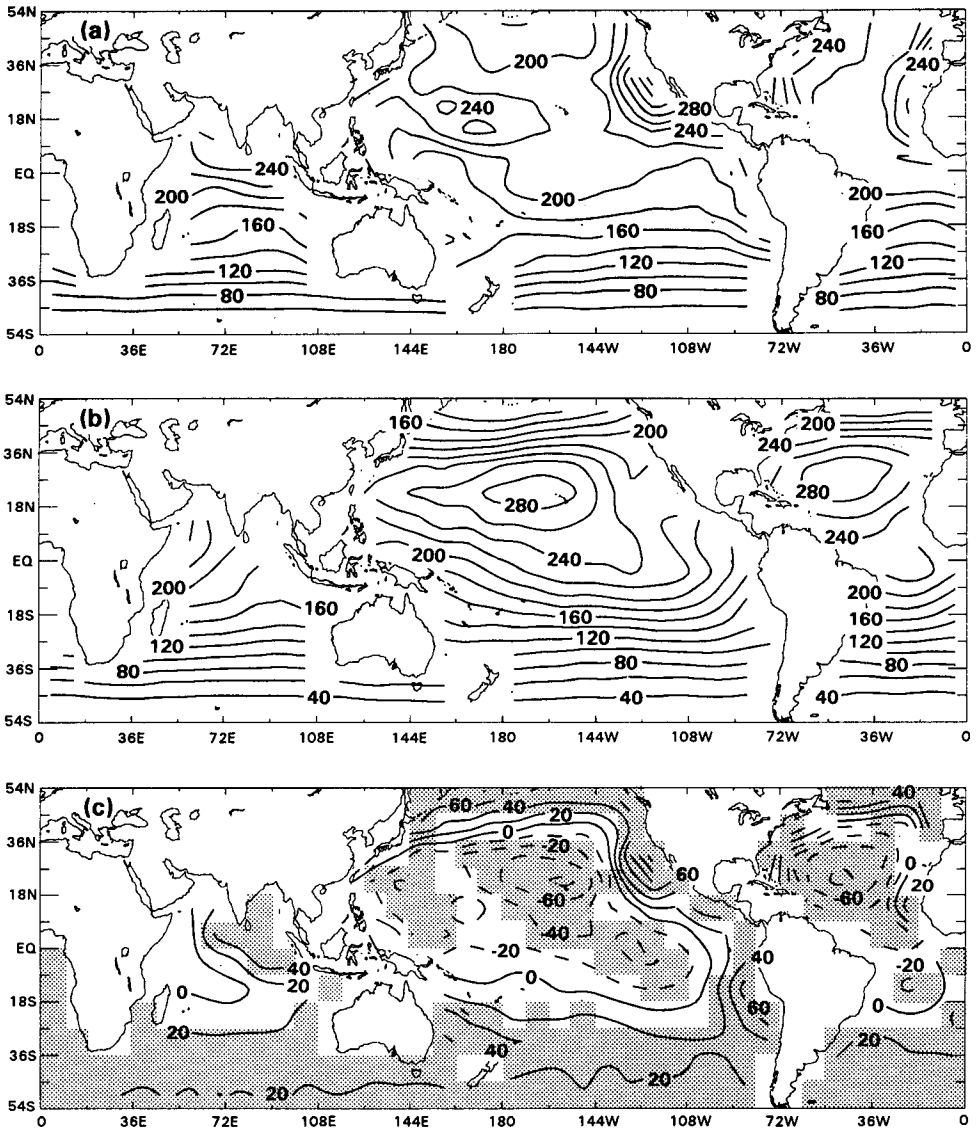

FIG. 2. As in Fig. 1 but for July climatologies.

with the condition that too much solar radiation is reflected and too little is transmitted to the surface and absorbed in the simulated system. In fact, the planetary albedo discrepancies are positive throughout the summer hemisphere in general, and the planetary albedo of the model is too high on global average. The areas of strong negative bias in ocean SSI do not extend across entire latitude bands, and therefore, the evidence of this bias is hidden to some extent in Figs. 3 and 5 because compensating regions of positive and negative bias both contribute to the zonal-mean computations.

The pattern of discrepancies between the GCM and satellite climatologies for July ocean SSI (Fig. 2c) shares common features with the pattern of discrepancies for January (Fig. 1c). Similar zonal gradients are found in the winter hemisphere extratropics in the GCM and satellite climatologies (Figs. 4 and 5), and GCM climatological values meet or exceed satellite climatological values (Figs. 2a and 2b, respectively). As in the January case, the GCM climatological values are less than the satellite climatological values in the summer hemisphere tropics (Fig. 2) by a statistically significant amount that reaches up to 80 W m^{-2}. Also, the discrepancies in the climatological values of planetary albedo are statistically significant and consistent with the SSI discrepancies. Again, the zonal-mean differences include regions of compensating positive and negative bias. Nevertheless, on zonal average (Figs. 4 and 5) a negative bias is clearly indicated for the summer hemisphere tropics. Discrepancies between the July climatologies in the summer hemisphere extratropics (Fig. 2c) are distinct from those in the January climatology

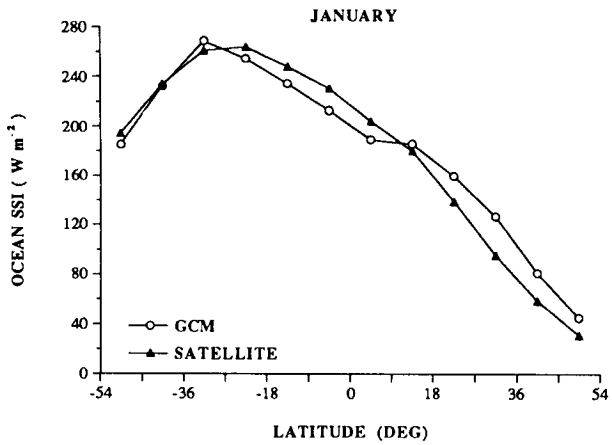

FIG. 3. The zonal mean of net surface solar irradiance (SSI) over the oceans (W m^{-2}) is shown as a function of latitude for the GLA GCM January climatology (circle symbol) and the satellite-based January climatology (triangle symbol).

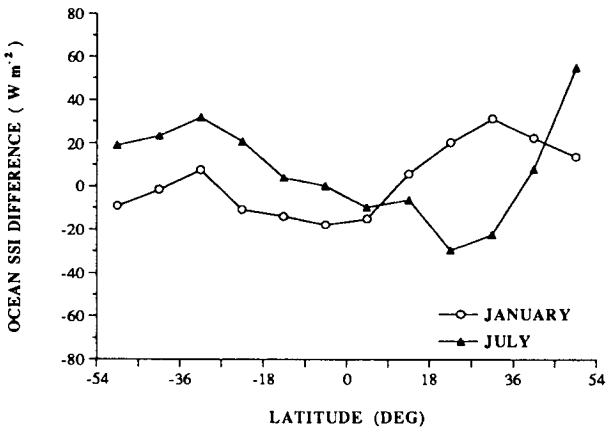

FIG. 5. The differences (W m^{-2}) between the zonal means of ocean SSI climatologies in the GLA GCM and satellite-based record for January (circle symbol) and July (triangle symbol). The satellite-based values are subtracted from the GCM values.

(Fig. 1c) in that a strong positive bias exists in the GCM values (Fig. 5). These positive discrepancies reach a maximum magnitude of 131 W m^{-2} off the western coast of North America. The associated discrepancies in planetary albedo reach their largest negative values indicating that too much solar radiation is reflected back to space by the planetary system in the model simulations.

5. Summary and conclusions

For the first time, a satellite-derived record of ocean SSI was used to assess the realism of ocean SSI simulated by the GLA GCM. January and July climatologies obtained from the 7-year satellite-based dataset were compared with the corresponding GCM climatologies. The GCM climatologies were computed from an ensemble of four 47-day simulations in each case. The results show that the GLA GCM has a positive bias (i.e., too much net SSI over the oceans in the model climatology) in the extratropics and a negative bias (i.e., too little net SSI over the oceans in the model climatology) in the tropics, especially in the summer hemisphere. Quantitative information about these biases is extremely important for diagnostic evaluations and development of cloud-radiation interaction parameterizations. Furthermore, future models addressing global change issues will couple AGCMs (atmospheric GCMs) with OGCMs (oceanic GCMs), and the net flux of solar radiation at the ocean surface, a vital driver of the OGCMs, is a critical parameter in the coupled model. It is therefore important that the latest-generation AGCMs produce realistic simulations of the net solar flux into the oceans.

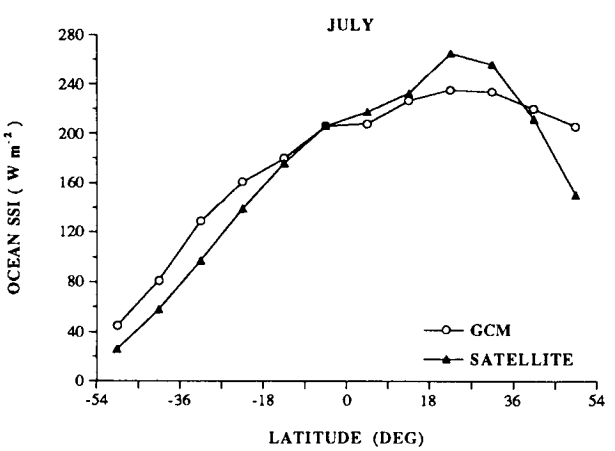

FIG. 4. As in Fig. 3 but for July climatologies.

Previously it has been shown that the synoptic-scale circulation of the GLA GCM is reasonable (Sud et al. 1990); therefore, the positive biases suggest cloud fractions that are too small or clouds that are optically too thin, whereas negative biases indicate cloud fractions that are too large or clouds that are optically too thick. The largest discrepancies between the GCM and satellite climatologies of ocean SSI, associated with consistent discrepancies in the planetary albedo climatologies, point to problems in the treatment of clouds. For example, GCM climatological values are much higher than satellite climatological values across the North Pacific, along the typical course of storm tracks. Even though a realistic number of migratory cyclones may be simulated, the radiative effect of the associated clouds is not being captured adequately and, consequently, there is too much SSI. There is also too much SSI in the July GCM simulations off the western coast of North America, presumably related to a deficiency in the ability of the model to reproduce the effects of the persistent marine stratus in this region without an explicit parameterization.

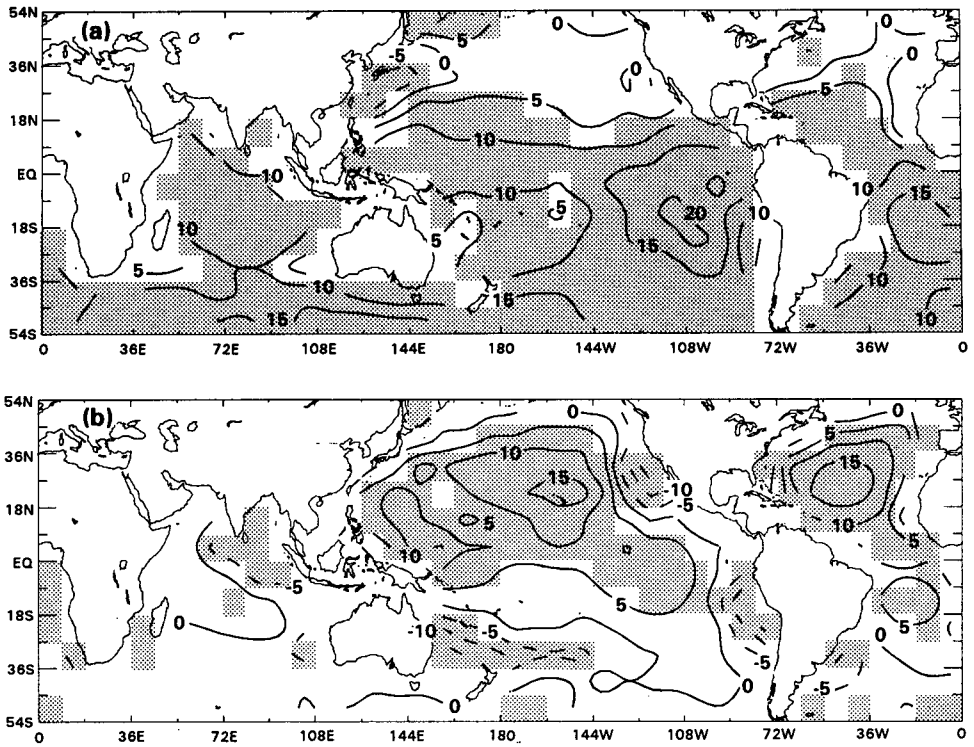

FIG. 6. The differences between the GLA GCM and satellite climatologies of planetary albedo (%) for (a) January and (b) July. The satellite values are subtracted from the GCM values. In both figures the contour interval is 5% and negative contours are dashed. Shading is used to indicate that the mean differences, scaled with the pooled variability of the ensemble, are significant at the 99% level according to the results of a Student's *t*-test.

Cloud–radiation interaction parameterizations in GCMs, although quite complex, are still relatively crude. Therefore, these GCM parameterizations are tuned, often in an ad hoc manner, to assure agreement with observed quantities on global and seasonal mean scales. It is hoped that the tuned parameters will have a realistic global distribution, but that does not follow automatically. The significance of the results presented here is that they clearly show regional and seasonal biases in a critical parameterization for investigations of global climate. The quantitative information in this study provides a bench mark for future evaluations and development of the GLA GCM.

REFERENCES

Arakawa, A., and W. H. Schubert, 1974: Interaction of a cumulus cloud ensemble with the large-scale environment, Part I. *J. Atmos. Sci.*, **31,** 674–701.

Arino, O., 1990: Albedo de surface et bilan radiatif de courtes longueurs d'ondes: Contribution satellitaire. Doctoral dissertation, Institut National Polytechnique de Toulouse, Toulouse, France, 205 pp.

Budyko, M. I., Ed., 1963: *Atlas Teplovogo Balansa Zemnogo Shara* [*Atlas of the Heat Balance of the Earth*], Karlfabrika Gosgeoltehizdata, 75 pp. [Also, *Guide to the Atlas of the Heat Balance of the Earth.* Translated by I. A. Donehoo, U.S. Weather Bureau, WB/T-106, 25 pp.]

Chertock, B., 1989: Global monitoring of net solar irradiance at the ocean surface using Nimbus-7 satellite data. Doctoral dissertation, Scripps Institution of Oceanography, University of California, San Diego, 118 pp.

——, R. Frouin, and R. C. J. Somerville, 1991: Global monitoring of net solar irradiance at the ocean surface: Climatological variability and the 1982–1983 El Niño. *J. Climate,* **4,** 639–650.

——, ——, and C. Gautier, 1992: A technique for global monitoring of net solar irradiance at the ocean surface. Part II: Validation. *J. Appl. Meteor.,* **31,** 1067–1083.

Chou, M.-D., 1986: Atmospheric solar heating rate in the water vapor bands. *J. Climate Appl. Meteor.,* **25,** 1532–1542.

Dorman, J. L., and P. J. Sellers, 1989: A global climatology of albedo, roughness length and stomatal resistance for atmospheric general circulation models as represented by the simple biosphere model (SiB). *J. Appl. Meteor.,* **28,** 833–855.

Esbensen, S. K., and Y. Kushnir, 1981: The heat budget of the global ocean: An atlas based on estimates from surface marine observations. Climatic Res. Inst. Rep. No. 29, 220 pp.

Frouin, R., and B. Chertock, 1992: A technique for global monitoring of net solar irradiance at the ocean surface. Part I: Model. *J. Appl. Meteor.,* **31,** 1056–1066.

Gautier, C., 1986: Evolution of the net surface shortwave radiation over the Indian Ocean during Summer MONEX (1979): A satellite description. *Mon. Wea. Rev.,* **114,** 525–533.

——, 1988: Surface solar irradiance in the central Pacific during Tropic Heat: Comparisons between in situ measurements and satellite estimates. *J. Climate,* **1,** 600–608.

——, G. Diak, and S. Masse, 1980: A simple physical model to estimate incident solar radiation at the surface from GOES satellite data. *J. Appl. Meteor.*, **19,** 1005–1012.

——, R. Frouin, B. Di Julio, and R. Wylie, 1986: Net solar irradiance at the ocean surface during Tropic Heat. California Space Institute CARS Rep. No. 014, 117 pp.

Hastenrath, S., and P. J. Lamb, 1978: *Heat Budget Atlas of the Tropical Atlantic and Eastern Pacific Oceans.* University of Wisconsin Press, 90 pp.

Hsiung, J., 1986: Mean surface energy fluxes over the global ocean. *J. Geophys. Res.*, **91,** 10 585–10 606.

Kalnay, E., R. Balgovind, W. Chao, D. Edelmann, J. Pfaendtner, L. Takacs, and K. Takano, 1983a: Documentation of the GLAS fourth order general circulation model. Vol. 1: Model documentation. NASA-TM-86064, Vol. 1; NAS 1.15:86064-Vol-1, NTIS, Washington, D.C., 381 pp.

——, ——, ——, ——, ——, ——, and ——, 1983b: Documentation of the GLAS fourth order general circulation model. Vol. 2: Scalar code. NASA-TM-86064, Vol. 2; NAS 1.15:86064-Vol-2, NTIS, Washington, D.C., 523 pp.

——, ——, ——, ——, ——, ——, and ——, 1983c: Documentation of the GLAS fourth order general circulation model. Vol. 3: Vectorized code for the Cyber 205. NASA-TM-86064, Vol. 3; NAS 1.15:86064-Vol-3, NTIS, Washington, D.C., 647 pp.

Kyle, H. L., P. E. Ardanuy, and E. J. Hurley, 1985: The status of the *Nimbus-7* earth-radiation-budget data set. *Bull. Amer. Meteor. Soc.*, **66,** 1378–1388.

Lacis, A., and J. E. Hansen, 1974: A parameterization for the absorption of solar radiation in the earth's atmosphere. *J. Atmos. Sci.*, **31,** 118–133.

Matsuno, T., 1966: A finite difference scheme for time integrations of oscillatory equations with second order accuracy and sharp cut-off for high frequencies. *J. Meteor. Soc. Japan,* **44,** 85–88.

Sellers, P. J., Y. Mintz, Y. C. Sud, and A. Dalcher, 1986: A simple biosphere model (SiB) for use within general circulation models. *J. Atmos. Sci.*, **43,** 505–531.

Slingo, J., and B. Ritter, 1985: Cloud prediction in the ECMWF model. Tech. Rep. No. 46. European Centre for Medium-Range Weather Forecasts, Reading, England, 49 pp.

Sud, Y. C., and A. Molod, 1988: The roles of dry convection, cloud-radiation feedback processes and the influence of recent improvements in the parameterization of convection in the GLA GCM. *Mon. Wea. Rev.*, **116,** 2366–2387.

——, P. J. Sellers, Y. Mintz, M. D. Chou, G. K. Walker, and W. E. Smith, 1990: Influence of the biosphere on the global circulation and hydrolic cycle—a GCM simulation experiment. *Agric. Forest Meteor.*, **52,** 133–180.

Weare, B. C., P. T. Strub, and M. D. Samuel, 1981: Annual mean surface heat fluxes in the tropical Pacific Ocean. *J. Phys. Oceanogr.*, **11,** 705–717.

Wu, M.-L. C., 1980: The exchange of infrared radiative energy in the troposphere. *J. Geophys. Res.*, **85,** 4084–4090.

Wyrtki, K., 1965: The average annual heat balance of the North Pacific Ocean and its relation to ocean circulation. *J. Geophys. Res.*, **70,** 4547–4559.

PAPERS TO APPEAR IN FORTHCOMING ISSUES

A Degeneracy in Cross-validated Skill in Regression-based Forecasts—ANTHONY G. BARNSTON AND HUUG M. VAN DEN DOOL, NWS/NMC/Climate Analysis Center, Washington, D.C.

A Teleconnection Study of Interannual Sea Surface Temperature Fluctuation in the Northern North Atlantic and Precipitation Runoff over Western Siberia—SHILING PENG AND LAWRENCE A. MYSAK, Centre for Climate and Global Change Research and Department of Atmospheric and Oceanic Sciences, McGill University, Montreal, Quebec, Canada.

Late Pleistocene Ice Age Scenarios Based on Observational Evidence—G. DEBLONDE, The Canada Center for Remote Sensing, Ottawa, Canada; AND W. R. PELTIER, Department of Physics, University of Toronto, Toronto, Ontario, Canada.

Effects of Weather Variability and Soil Parameter Uncertainty on the Soil–Crop–Climate System—ANGELOS L. PROTOPAPAS, Polytechnic University, Brooklyn, New York; AND RAFAEL L. BRAS, Massachusetts Institute of Technology, Cambridge, Massachusetts.

Estimation of the Fractional Coverage of Rainfall in Climate Models—E. A. B. ELTAHIR AND R. L. BRAS, Ralph M. Parsons Laboratory, Massachusetts Institute of Technology, Cambridge, Massachusetts.

Aperiodic Variability in the Cane–Zebiak Model: A Diagnostic Study—B. N. GOSWAMI, Centre for Atmospheric Sciences, Indian Institute of Science, Bangalore, India; AND J. SHUKLA, Center for Ocean–Land–Atmosphere Interactions, Department of Meteorology, University of Maryland, College Park, Maryland.

Impacts of Severe Winter Weather during December 1989 in the Lake Erie Snowbelt—THOMAS W. SCHMIDLIN, Department of Geography, Water Resources Research Institute, Kent State University, Kent, Ohio.

Further Work on the Prediction of Northeast Brazil Rainfall Anomalies—STEFAN HASTENRATH AND LAWRENCE GREISCHAR, Department of Meteorology, University of Wisconsin—Madison, Madison, Wisconsin.

An Accurate Parameterization of the Radiative Propeties of Water Clouds Suitable for Use in Climate Models—Y. X. HU AND K. STAMNES, Geophysical Institute and Department of Physics, University of Alaska—Fairbanks, Fairbanks, Alaska.

An Assessment of Low-Frequency Variability in the Tropics as Indicated by Some Proxies of Tropical Convection—PRASHANT D. SARDESHMUKH AND BRANT LEIBMANN, Cooperative Institute for Research in the Environmental Sciences, University of Colorado, Boulder, Colorado.

The 200-mb Climatological Vorticity Budget during 1986–1989 as Revealed by NMC Analyses—KINGTSE MO, Climate Analysis Center, NMC/NWS/NOAA, Washington, D.C.; AND EUGENE M. RASMUSSON, Cooperative Institute of Climate Studies, Department of Meteorology, University of Maryland, College Park, Maryland.

Linkages between 200-mb Tropical and Extratropical Circulation Anomalies during the 1986–1989 ENSO Cycle—EUGENE M. RASMUSSON, Cooperative Institute of Climate Studies, Department of Meteorology, University of Maryland, College Park, Maryland; AND KINGTSE MO, Climate Analysis Center, NMC/NWS/NOAA, Washington, D.C.

Structure of Oceanic and Atmospheric Low-Frequency Variability over the Tropical Pacific and Indian Oceans. Part I: COADS Observations—SUMANT NIGAM AND HORNG-SYI SHEN, Center for Ocean–Land–Atmosphere Interactions, Department of Meteorology, University of Maryland, College Park, Maryland.

Structure and Predictability of the El Niño/Southern Oscillation Phenomenon in a Coupled Ocean–Atmosphere General Circulation Model—M. LATIF, A. STERL, E. MAIER-REIMER, AND M. M. JUNGE, Max-Planck-Institut für Meteorologie, Hamburg, Germany.

Case Studies of Extreme Climatic Events in the Amazon Basin—JOSE A. MARENGO AND STEFAN HASTENRATH, Department of Meteorology, University of Wisconsin—Madison, Madison, Wisconsin.

Intraseasonal Oscillations over the Atlantic—LLOYD J. SHAPIRO AND STANLEY B. GOLDENBERG, Hurricane Research Division/ Atlantic Oceanographic and Meteorological Laboratory, Miami, Florida.

The Joint Modes of the Coupled Atmosphere–Ocean System Observed from 1967 to 1986—JIN-SONG XU, Max-Planck-Institut für Meteorologie, Hamburg, Germany.

Sensitivity of Dynamical Quantities to Horizontal Resolution for a Climate Simulation Using the ECMWF (Cycle 33) Model—JAMES S. BOYLE, Program for Climate Model Diagnosis and Intercomparison, Lawrence Livermore National Laboratory, Livermore, California.

Correlation Dimensions of Local, Short-Term Climatic Attractors from Observations and a Global Climate Model—HOWARD W. BARKER, Atmospheric Environment Service, Canadian Climate Centre, Downsview, Ontario, Canada; AND BRANDON VAN ZYL, Department of Physics, McLennan Physical Laboratory, University of Toronto, Toronto, Ontario, Canada.

Scaling Water and Energy Fluxes in Climate Systems: Three Land–Atmospheric Modeling Experiments—ERIC F. WOOD AND VENKATARAMAN LAKSHMI, Water Resources Program, Princeton University, Princeton, New Jersey.

Global Warming and the Problem of Testing for Trend in Time Series Data—WAYNE A. WOODWARD AND H. L. GRAY, Department of Statistical Science, Southern Methodist University, Dallas, Texas.

Interannual Variability in Mediterranean Heat and Bouyancy Fluxes—CHRIS GARRETT, RICHARD OUTERBRIDGE, Centre for Earth and Ocean Research, University of Victoria, Victoria, British Columbia, Canada; AND KEITH THOMPSON, Department of Oceanography, Dalhousie University, Halifax, Nova Scotia, Canada.

Interannual Variability of the Onset of the Indian Summer Monsoon and Its Association with Atmospheric Features, El Niño, and Sea Surface Temperature Anomalies—PORATHUR V. JOSEPH, JON K. EISCHEID, AND ROBERT J. PYLE, Cooperative Institute for Research in Environmental Sciences, University of Colorado, Boulder, Colorado.

Mesoscale Convective Complexes over the Indian Monsoon Region—ARLENE G. LAING AND J. MICHAEL FRITSCH, Department of Meteorology, The Pennsylvania State University, University Park, Pennsylvania.

Impact of Mount Pinatubo Aerosols on Satellite-derived Sea Surface Temperatures—RICHARD W. REYNOLDS, National Meteorological Center, National Weather Service, National Oceanic and Atmospheric Administration, Washington, D.C.

A Dynamical Interpretation of the Global Response to Equatorial Pacific Sea Surface Temperature Anomalies—FRANCO MOLTENI, LAURA FERRANTI, T. N. PALMER, AND PEDRO VITERBO, European Centre for Medium-Range Weather Forecasts, Reading, Berkshire, United Kingdom.

Annual Cycle of Equatorial East–West Circulation over the Indian and Pacific Oceans—TAKIO MURAKAMI AND BIN WANG, Department of Meteorology, School of Ocean and Earth Science and Technology, University of Hawaii, Honolulu, Hawaii.

Observations of Seasonal Variations in Atmospheric Greenhouse Trapping and Its Enhancement at High Sea Surface Temperature—ROBERT HALLBERG, School of Oceanography, University of Washington, Seattle, Washington; AND ANAND INAMDAR, California Space Institute, Scripps Institution of Oceanography, La Jolla, California.

Uncertainties in Climatological Tropical Humidity Profiles: Some Implications for Estimating the Greenhouse Effect—DAVID S. GUTZLER, Atmospheric and Environmental Research, Inc., Cambridge, Massachusetts.